島根大学地球資源環境学研究報告　22, 121～133 ページ（2003 年 12 月）
Geoscience Rept. Shimane Univ., 22, p.121～133（2003）

Article

Hydrothermal alteration at Crater Mountain, Papua New Guinea: Evidence from alteration mineral chemistry and lithogeochemistry

Shadrach K. Noku*, Masahide Akasaka* and Barry P. Roser*

Abstract

The Crater Mountain district of Papua New Guinea has been explored for precious metals since 1970. The latest phase saw the completion of seven exploration drill holes in 1999. The drill core consists of feldspar andesite, feldspar diorite, quartz-feldspar porphyry, hornblende-feldspar porphyry, lithic tuff, pyroclastics/breccia, and mud/siltstone. Hydrothermal alteration of these lithotypes has developed mineral assemblages composed of K-mica, carbonate (dolomite, ankerite, magnesite, and magnesian siderite), chlorite and pyrite. The abundance of hydrothermal chlorite is greater in the volcanic lithotypes, whereas K-mica (sericite), carbonate and quartz pseudomorphs are common in the intrusive rocks, particularly replacing primary ferromagnesian minerals. Accessory apatite and zircon are the only minerals which survive hydrothermal alteration. Fe and Mg contents of K-mica decrease with increasing alteration (chloritization) representing changes in Na content to muscovite/sericite (K).

Immobile trace element ratios (Zr/TiO_2-Nb/Y) indicate most samples were originally of trachyandesite composition. All samples are hydrothermally altered to some degree and are enriched in SiO_2, K_2O, and Rb, and are depleted in CaO, Na_2O, MgO, Ba, and Sr. Elevated concentrations of MgO, Fe_2O_3 and K_2O coupled with low Na_2O and CaO values characterize chloritization. The pattern of low Na_2O, CaO and MgO values and high K_2O values are indicative of chlorite-sericite ± quartz alteration. Values of the Ishikawa alteration index (AI) and the chlorite-carbonate-pyrite index (CCPI) become progressively greater passing from relatively less altered samples (AI = 51–61; CCPI = 62–66) to strongly altered samples (AI = 42–98; CCPI = 18–99). Zn is often elevated at AI values between 50 and 90, whereas Zn and As are enriched in samples with CCPI values between 55 and 75. Sr/Ba ratios are lowest at AI values above 90. The geochemical halo patterns and alteration mineral chemistry reflect the composite response of lithofacies to mineralogical and textural changes accompanying hydrothermal alteration associated with ore emplacement.

Key words: hydrothermal alteration, Crater Mountain, Papua New Guinea

Introduction

The Crater Mountain prospect is located at an elevation of about 3, 100 m in mountainous terrain in central Papua New Guinea. It was formed during Early Pliocene collision between the northeastern margin of the Australasian plate and an island arc located on the Bismarck Sea plate (Hall, 1994; Fig.1A). Crater Mountain has been the target of exploration for precious metals since 1970. Several companies have worked in the area, and extensive reports of their operations are available. These cover stream sediment analyses, trenching, rock chip data, aerial imagery and magnetic data.

The most recent development in the area was completion of seven drill holes (Fig. 1B) by BHP and Macmin N.L in 1999. Assay data for precious metals are available for all seven holes, but no detailed petrography and geochemical data were reported for the wall rocks. Pile and Philip (1995, 1996) and Gilbert (1996) carried out petrological description of rock chip samples from the Nevera and Nimi areas within Crater Mountain, and Pertzel (1998) made petrographic descriptions of five drill core samples from Nevera.

*Dept. of Geoscience, Shimane University, Matsue 690-8504, Japan

Geochemical data for some volcanic and intrusive rocks from the Papua New Guinea Highlands can be found in Mason and McDonald (1978) and Johnson (1982). Richards (1990) reported on the petrology and geochemistry of alkalic intrusives at the Porgera gold deposit.

Study of the geochemistry and alteration mineral chemistry of the wall rocks of ore prospects are of critical importance, because an understanding of their relationship can lead to improved targeting of mineralized zones within complex hydrothermal alteration systems. Studies of the relationship between alteration mineralogy and lithogeochemistry associated with different types of deposit are usually carried out with this in mind (e.g. Ishikawa, et al., 1976; Large, et al., 2001; Doyle, 2001). Here we report the first geochemical data for the wall rocks at Crater Mountain, based on 32 samples, combined with electron microprobe analyses of alteration minerals.

Local Geology

Several volcanic units of andesitic to dacitic composition were noted in the area during creek mapping and from petrology by previous workers (e.g. Pile and Philip, 1995; 1996; Gilbert, 1996). The tuffaceous units include crystal lithic tuff, ash fall tuff, and lapilli/lithic tuff. The porphyritic

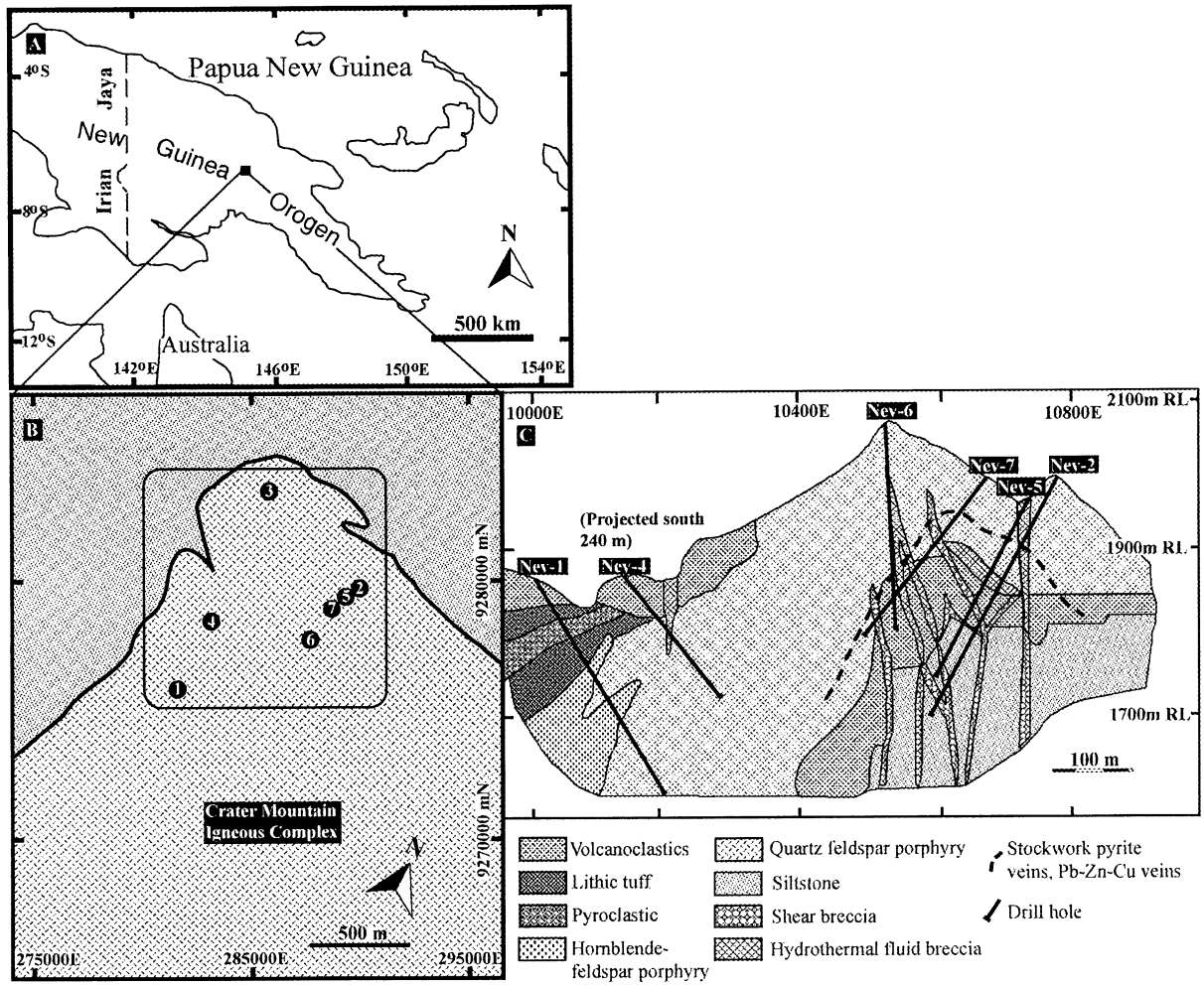

Fig. 1. (A) Locality of the Crater Mountain deposit. (B) Local geology of the Nevera area, Crater Mountain, showing the locations of seven bore holes. (C) Bore hole cross section from Nev-2 to Nev-1. The dashed line defines the zone of the pyrite-base metal stockwork. Simplified from Macmin, annual company report (1999).

units comprise trachyandesite, quartz diorite porphyry, andesite porphyry, diorite porphyry, feldspar porphyry and quartz biotite porphyry. Hornblende feldspar porphyry intrudes quartz feldspar porphyry and the overlying volcanic units (Fig. 1C). Grey mudstones and siltstones are in contact with the volcanics in the northwest and north of the area. These are overlain by volcanics and quartz feldspar porphyry. Hydrothermal and shear breccias cut the mudstone/siltstone unit and extend into the overlying volcanics and quartz feldspar porphyry (Fig. 1C). These breccias contain clasts of mudstone, siltstone, porphyritic lithotypes, and volcanics.

Alteration is widespread, with clay-pyrite alteration in the north grading into chlorite ≫ clay > carbonate to the southeast, south and southwest. Base metal (galena/sphalerite) veining is common throughout the area (Pile and Philip, 1995; 1996). Three alteration assemblages have been identified in the area. These are calcite-sericite-chlorite, chlorite-sericite and quartz-sericite (Noku, 2003).

Structures in the area are not well defined due to the thick volcanic and vegetation cover present, but preliminary interpretation of ground magnetic data identified several structures trending NW–SE and NE–SW (Pile and Philip, 1995; 1996).

Sampling and Analytical Methods

The initial plan for sampling in this study was to make detailed description of the seven drill cores stored at the exploration camp site, and to collect representative core sections for laboratory work. However, the cores were trashed before that sampling could be carried out. Consequently, representative samples were collected from the dumped core based on their lithology, alteration, mineralogy, texture, and structure. The samples collected represent all lithotypes intersected by the drill holes (Fig. 1 C), including breccias and stockwork pyrite veins. The siltstone (mudstone) unit occurs at depth, and was intersected by holes Nev-2 and Nev-5. The volcanics occur at the surface, and also overlain by quartz-feldspar

porphyry, which is the dominant lithology. Hornblende-feldspar porphyry (possibly a dike) intrudes quartz-feldspar porphyry and the overlying volcanics.

Petrology and EPMA Analysis

More than 60 polished thin-sections were prepared from all rock types for petrographic examination. Identification of ore and gangue minerals were conducted using reflected light and transmitted light microscopy respectively. Based on the petrography, selected samples were carbon-coated under vacuum for subsequent electron microprobe analysis (EPMA). The instrument used was a JXA-8800 M. Sulfides were analyzed using operating conditions of 20 kV accelerating voltage, 20 nA beam current, 20 seconds peak acquisition times and 2–3 μm probe diameter. For silicate minerals, the accelerating voltage was set at 15 kV. In addition to petrography, X-ray powder diffraction method (XRD) was applied to 17 powdered samples to identify clay (alteration) minerals present and their relative abundances.

XRF analysis

Thirty two samples of the volcanics, intrusives and mudstone were crushed in a tungsten carbide ring mill and oven dried at 110°C. LOI (loss of ignition) was determined by ignition of oven-dried sample in a muffle furnace at 1000°C for four hours. XRF analyses were carried out using a RIGAKU RIX-2000 X-ray fluorescence spectrometer, on both glass discs and pressed powder pellets. The glass beads were prepared from the ignited samples, using an alkali flux consisting of 80% lithium tetraborate and 20% lithium metaborate, with a sample to flux ratio of 1:2, following the method of Kimura and Yamada (1996). These beads were used to determine major elements and 13 trace elements (Ba to Zr; Table 1). Pressed powder pellets were prepared from unignited powder (hydrous basis) for the analysis of As, Zn, Cu, U, S, and Sc. The XRF analyses were made to classify the rock types, and to determine element mobility (degree of alteration).

Results and Discussion

Alteration mineral chemistry

The compositions of altered and unaltered phases were determined by EPMA, including chlorite, sericite, carbonate, diaspore and apatite. Only the results for chlorite, K-mica (sericite) and carbonate (Tables 1 to 3) are discussed here, as they comprise alteration minerals.

Chlorite

Chlorite occurs in the wall rocks as a hydrothermal alteration replacement of ferro-magnesian minerals. It also occurs in veins, where it exhibits fibrous platy texture. On a chlorite classification diagram (Fig. 2), the analyzed chlorites have quite uniform Fe/(Fe + Mg + Mn) ratios, mainly lying across the fields of the magnesian chlorites

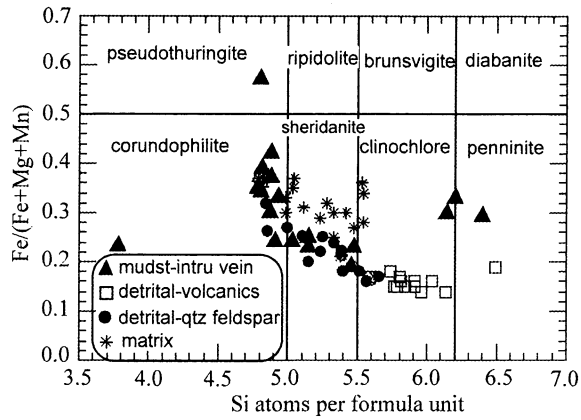

Fig. 2. Compositions of chlorite from wall rocks and veins on a chlorite classification diagram after Foster (1962), derived from EPMA analyses. Exsolved muscovite chlorite alteration of detrital muscovite grains. Abbreviations: mst-intru = mudstone-intrusive, and qtz = quartz.

(clinochlore, sheridanite and corundophilite). Chlorites occurring in veins show great variation in Si content and one analysis has a high Fe/(Fe + Mg + Mn) ratio, whereas analyses of chlorites in the matrix and those replacing detrital muscovite grains within the same samples have compositions similar to each other. The considerable variation in silica for hydrothermal chlorites suggests differing genetic conditions (i.e. temperature of formation, fluid chemistry; Noku, 2003).

K-mica

EPMA analyses of detrital muscovite and sericite (fine-grained muscovite) in the matrix are presented in Table 2. The K-mica compositions show a trend of increasing Al^{VI} and decreasing iron and magnesium with increasing silica (Fig. 3). When related to mode of occurrence, platy K-mica has greater iron and magnesium contents than does the fibrous matrix K-mica. The plots also show that the matrix K-mica is less phengitic than the detrital K-mica.

Carbonate

Carbonate minerals are present in the wall rocks predominantly as replacements of feldspar and chlorite, but are also found as patches in the matrix and infilling cavities. They also occur as carbonate veins associated with sulfides and in breccias. Most of the carbonate minerals analyzed by EPMA were restricted to dolomite-ankerite, although a few analyses reflect calcite, ferroan magnesite, and magnesian siderite compositions (Table 3, Fig. 4). Following Buckley and Woolley (1990), the boundary between dolomite and ankerite is taken at an Fe:Mg ratio of 1:4, and the magnesite -siderite series is subdivided at Mg:Fe ratios of 0.75, 0.5 and 0.25 into magnesite and ferroan magnesite.

The vein samples show compositional variation from dolomite to ankerite, whereas carbonate replacements of feldspar and chlorite range through ankerite-dolomite-

Table 1. Selected EPMA analyses of chlorite from altered wall rocks and fractures. Analyses 1–4 are from volcanic tuff, 5–8 are from fractures between intrusive-mudstone contacts, and 9–11 are from quartz-feldspar porphyry.

An. No.	*1*	*2*	*3*	*4*	*5*	*6*	*7*	*8*	*9*	*10*	*11*
SiO_2	26.67	25.50	29.43	27.83	24.41	24.15	26.77	26.63	30.24	30.55	30.49
TiO_2	0.00	0.01	0.02	0.00	0.04	0.02	0.07	0.02	0.04	0.04	0.01
Al_2O_3	20.88	22.94	20.80	20.79	23.52	25.24	23.54	23.90	20.85	21.37	21.53
Cr_2O_3	0.00	0.20	0.00	0.00	0.00	0.00	0.01	0.00	0.01	0.00	0.01
V_2O_3	0.03	0.15	0.01	0.00	0.02	0.06	0.12	0.00	0.07	0.01	0.07
FeO	15.24	16.04	10.55	11.45	21.04	18.92	14.74	13.29	10.69	9.64	8.73
MnO	2.72	1.25	0.43	0.85	0.27	0.21	0.19	0.18	1.30	1.43	1.34
MgO	21.80	21.15	26.68	25.68	18.33	17.75	22.30	22.85	24.51	23.87	25.12
CaO	0.03	0.01	0.05	0.00	0.02	0.01	0.05	0.08	0.11	0.10	0.06
Na_2O	0.01	0.00	0.01	0.00	0.00	0.01	0.00	0.01	0.02	0.06	0.00
K_2O	0.00	0.00	0.00	0.00	0.00	0.00	0.00	0.00	0.09	0.65	0.30
P_2O_5	0.00	0.01	0.00	0.00	0.00	0.03	0.00	0.00	0.02	0.05	0.02
Total	87.38	87.26	87.98	86.60	87.65	86.40	87.79	86.96	87.95	87.77	87.68
Number of ions on the basis of 28 oxygens											
Si	5.25	5.00	5.58	5.40	4.82	4.79	5.15	5.15	5.74	5.81	5.77
Al^{IV}	2.75	3.00	2.43	2.60	3.18	3.21	2.85	2.85	2.26	2.19	2.23
Al^{VI}	2.09	2.31	2.22	2.15	2.29	2.70	2.49	2.59	2.41	2.59	2.58
Ti	0.00	0.00	0.00	0.00	0.01	0.00	0.01	0.00	0.01	0.01	0.00
Cr	0.00	0.03	0.00	0.00	0.00	0.00	0.00	0.00	0.00	0.00	0.00
V	0.01	0.02	0.00	0.00	0.00	0.01	0.02	0.00	0.01	0.00	0.01
Fe	2.26	2.37	1.50	1.67	3.13	2.83	2.14	1.93	1.53	1.38	1.24
Mn	0.45	0.21	0.07	0.14	0.05	0.04	0.03	0.03	0.21	0.23	0.22
Mg	6.39	6.19	7.54	7.43	5.40	5.25	6.40	6.59	6.94	6.77	7.09
Ca	0.01	0.00	0.01	0.00	0.00	0.00	0.01	0.02	0.02	0.02	0.01
Na	0.00	0.00	0.01	0.00	0.00	0.01	0.00	0.00	0.01	0.02	0.00
K	0.00	0.00	0.00	0.00	0.00	0.00	0.00	0.00	0.02	0.16	0.07
P	0.00	0.00	0.00	0.00	0.00	0.01	0.00	0.00	0.00	0.01	0.00
Total	19.21	19.13	19.36	19.39	18.88	18.85	19.10	19.16	19.16	19.19	19.22

Table 2. Selected EPMA analyses of K-mica from altered wall rocks and fractures. Analyses 1–5 represent detrital grains, 6–9 are from matrix and 10–11 are from a fracture.

An. No.	*1*	*2*	*3*	*4*	*5*	*6*	*7*	*8*	*9*	*10*	*11*
SiO_2	45.69	49.56	48.34	47.42	45.94	46.19	49.48	49.96	46.82	48.62	48.96
TiO_2	0.19	0.14	1.37	0.16	0.22	0.08	0.05	0.24	0.22	0.08	0.10
Al_2O_3	34.86	36.23	35.80	37.50	34.91	33.95	34.98	34.94	35.76	36.52	38.01
Cr_2O_3	0.00	0.00	0.04	0.03	0.02	0.02	0.02	0.02	0.01	0.00	0.00
V_2O_3	0.00	0.02	0.13	0.07	0.10	0.06	0.03	0.04	0.04	0.02	0.14
FeO	0.97	0.73	0.21	0.30	0.25	1.32	0.73	0.52	0.67	0.63	0.80
MnO	0.25	0.07	0.05	0.00	0.00	0.10	0.00	0.11	0.00	0.02	0.06
MgO	2.64	1.59	1.52	1.12	1.63	7.59	0.66	2.47	1.62	0.63	0.41
CaO	0.03	0.16	0.00	0.02	0.03	0.01	0.19	0.06	0.06	0.09	0.29
Na_2O	0.22	0.33	0.31	0.64	0.29	0.19	0.57	0.52	1.02	0.15	0.69
K_2O	9.22	9.67	9.98	9.09	10.36	5.41	6.92	9.72	9.24	7.30	7.85
Total	94.07	98.50	97.75	96.35	93.75	94.92	93.63	98.60	95.46	94.06	97.31
Number of ions on the basis of 22 oxygens											
Si	6.10	6.29	6.20	6.14	6.17	6.01	6.48	6.34	6.15	6.35	6.22
Al^{IV}	1.90	1.71	1.80	1.86	1.83	1.99	1.52	1.66	1.85	1.65	1.78
Al^{VI}	3.59	3.71	3.61	3.86	3.70	3.21	3.88	3.57	3.69	3.97	3.92
Ti	0.02	0.01	0.13	0.02	0.02	0.01	0.01	0.02	0.02	0.01	0.01
Al	5.49	5.42	5.41	5.72	5.53	5.20	5.40	5.23	5.54	5.62	5.69
Cr	0.00	0.00	0.00	0.00	0.00	0.00	0.00	0.00	0.00	0.00	0.00
V	0.00	0.00	0.01	0.01	0.01	0.01	0.00	0.00	0.00	0.00	0.02
Fe	0.10	0.07	0.02	0.03	0.03	0.13	0.07	0.05	0.07	0.06	0.08
Mn	0.03	0.01	0.01	0.00	0.00	0.01	0.00	0.01	0.00	0.00	0.01
Mg	0.53	0.30	0.29	0.22	0.33	1.47	0.13	0.47	0.32	0.12	0.08
Ca	0.01	0.02	0.00	0.00	0.00	0.00	0.03	0.01	0.01	0.01	0.04
Na	0.06	0.08	0.08	0.16	0.08	0.05	0.15	0.13	0.26	0.04	0.17
K	1.57	1.57	1.63	1.50	1.78	0.90	1.16	1.58	1.55	1.22	1.27
Total	19.40	19.19	19.19	19.52	19.48	18.99	18.83	19.07	19.46	19.05	19.29

Table 3. Representative EPMA analyses of carbonate minerals from altered wall rock and sulfide veins. Analyses 1–5 are from carbonate in sulfide veins, 6–7 are euhedral grains in cavities, and 8–11 are from replacements.

An. No.	*1*	*2*	*3*	*4*	*5*	*6*	*7*	*8*	*9*	*10*	*11*
FeO	0.31	0.60	0.94	9.21	6.71	34.90	22.97	0.23	0.00	0.00	1.35
MgO	17.94	18.03	21.78	18.56	21.55	15.29	24.96	0.29	0.36	0.38	23.50
CaO	29.90	27.94	28.83	24.77	27.70	4.56	2.78	57.23	73.36	72.33	31.24
MnO	6.41	13.96	10.26	2.60	2.68	4.09	3.07	4.46	0.46	0.79	0.16
Total	54.56	60.53	61.81	55.14	58.64	58.84	53.78	62.21	74.18	73.50	56.25
Number of ions on the basis of 6 oxygens											
Fe	0.02	0.04	0.06	0.62	0.42	2.22	1.50	0.02	0.00	0.00	0.09
Mg	2.48	2.31	2.66	2.47	2.67	1.93	3.24	0.04	0.04	0.04	3.00
Ca	2.97	2.58	2.53	2.37	2.47	0.41	0.26	5.56	5.91	5.89	2.86
Mn	0.50	1.02	0.71	0.20	0.19	0.29	0.23	0.34	0.03	0.05	0.01
Total	5.97	5.95	5.96	5.66	5.75	4.85	5.23	5.96	5.98	5.98	5.96

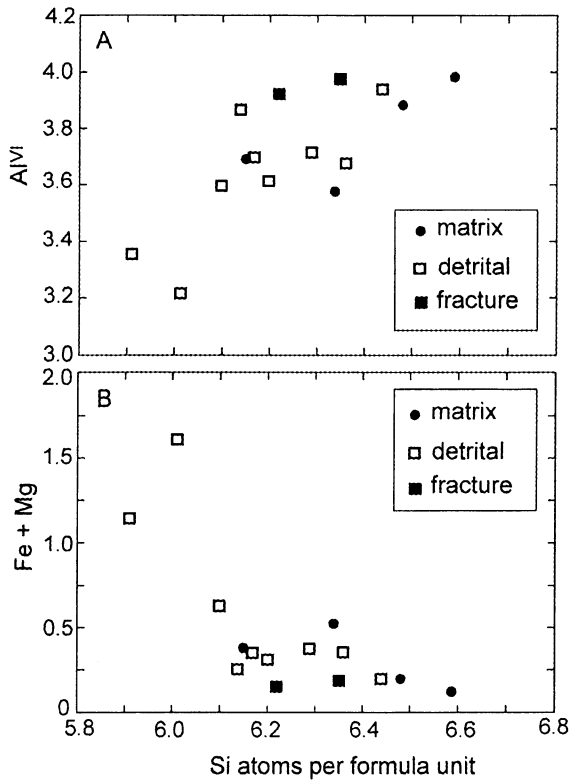

Fig. 3. Compositions of K-mica in wall rocks and fractures for (A) Si vs. Al^{VI} and (B) Si vs. Fe + Mg, derived from EPMA analyses.

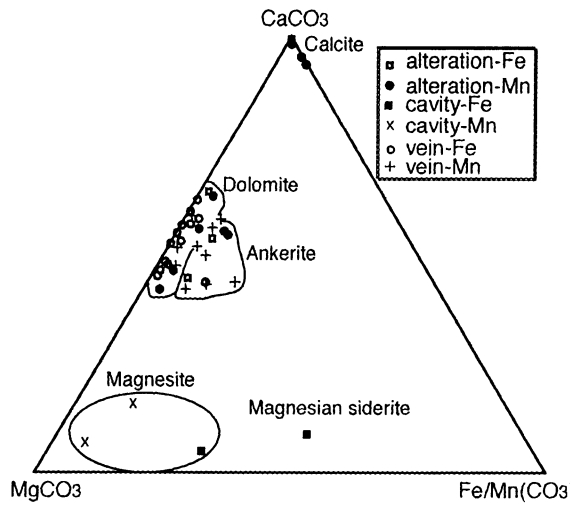

Fig. 4. Ternary plot of carbonate compositions calculated from EPMA analyses (Table 3) in samples of wall rocks and veins. All samples have compositions in the dolomite-ankerite range, except for a few in the calcite and magnesite-magnesian siderite series. Fe and Mn contents were used for discriminating $FeCO_3$ and $MnCO_3$ carbonates.

calcite. Carbonate in cavities span a wide range of composition from ferroan magnesite to magnesian siderite (Fig. 4). The paragenesis for carbonate associated with gold -bearing veins shows a sequence from Mn-rich to Fe-poor carbonate through the series dolomite-ankerite-calcite.

Lithogeochemistry

Major and trace element analyses of the drill core samples are listed in Table 4. The composition of these samples varies widely, indicating that most major elements and some trace elements were mobile during alteration. Loss on ignition (LOI) shows significant variation, with the more altered rocks having higher LOI values relative to the least altered samples. The higher LOI values mainly reflect the increase in volatile components (H_2O, CO_2 and S) resulting from the formation of hydrothermal muscovite/ sericite, carbonate and pyrite in the altered rocks. SiO_2 contents range from 52.12 to 72.88 wt%, and abundances of the mobile elements MgO, CaO, Na_2O and K_2O range from near zero to maximums of 7.73, 3.95, 2.76, and 4.68 wt%, respectively (Table 4). With the exception of a few isolated values, TiO_2, Al_2O_3 and Fe_2O_3 show considerably less variation. Trace element abundances also show extreme variability, with minimum values of all elements except Ba, Ce, Nb, V, and Zr lying near the lower limits of detection. Maximum values of economically significant elements are elevated well beyond levels expected for unmineralized

Table 4. Major and trace element analyses of drill core samples from Crater Mountain, reported on a hydrous basis.

SaNr	NR1	NR2	NR3	NR4	NR5	NR6	NR7	NR8	NR9	NR10	NR11	NR12	NR13	NR14	NR15	NR16	NR17	NR18	NR19	NR20	NR21	NR22	NR23	NR24	NR25	NR26	NR27	NR28	NR29	NR30	NR31	NR32
Lithology	And	And	And	And	And	And	And	And	And	And	And	And	Dior	Dior	Dior	Dior	Prph	Prph	Prph	Prph	Prph	Prph	Tuff	Tuff	Tuff	Tuff	Tuff	Tuff	Pyrc	Pyrc	Pyrc	Mst
Major elements (wt%)																																
SiO_2	70.77	65.98	62.05	62.48	72.88	62.57	59.55	64.40	63.87	66.89	69.93	68.06	67.51	66.43	64.65	65.33	65.84	61.62	63.69	62.94	63.65	63.62	61.80	54.17	63.33	52.12	67.51	64.56	71.21	70.33	62.20	62.16
TiO_2	0.57	0.54	0.67	0.58	0.54	0.53	0.55	0.49	0.71	0.44	0.54	0.51	0.46	0.54	0.47	0.48	0.65	0.47	0.49	0.53	0.53	0.44	0.60	1.64	0.58	1.60	0.50	0.57	0.56	0.64	0.51	0.95
Al_2O_3	14.86	16.31	14.55	16.59	14.49	16.26	16.01	15.10	17.20	15.95	13.50	16.68	16.43	16.95	15.04	16.13	17.28	14.90	16.06	16.31	16.29	15.62	16.46	16.45	16.88	15.89	16.27	15.21	17.62	15.23	15.87	18.54
Fe_2O_3	6.52	4.84	6.61	6.34	5.76	7.02	6.53	7.38	5.70	4.81	4.48	4.06	5.31	6.29	8.84	5.10	5.14	4.28	4.80	6.32	5.91	5.59	8.12	7.17	6.76	8.90	7.67	6.00	5.51	0.69	10.20	6.55
MnO	0.01	0.30	0.29	0.30	0.01	0.13	0.23	0.18	0.02	0.03	0.02	0.23	0.01	0.01	0.01	0.12	0.04	0.38	0.19	0.45	0.11	0.18	0.09	0.36	0.17	0.34	0.01	0.14	0.00	0.01	0.01	0.02
MgO	0.49	2.54	2.40	4.26	0.44	1.98	1.96	2.23	2.47	2.79	0.51	1.97	0.58	0.31	0.49	1.67	2.32	2.29	2.77	2.70	2.50	2.39	1.84	6.11	2.60	7.73	0.42	2.06	0.04	0.11	0.35	1.49
CaO	0.05	0.44	2.75	0.17	0.05	0.77	3.11	0.23	0.57	0.28	0.05	1.36	0.21	0.05	0.05	0.70	0.42	3.00	2.16	0.71	1.00	0.85	0.39	2.29	0.36	3.95	0.21	0.31	0.13	0.06	0.22	0.42
Na_2O	0.08	0.05	1.23	0.09	0.09	0.16	0.42	0.08	0.86	0.22	0.02	0.09	0.30	0.07	0.10	0.01	0.56	0.11	2.41	0.70	2.76	2.32	0.23	0.10	1.56	0.17	0.32	0.21	0.00	0.07	0.18	0.26
K_2O	3.91	3.52	2.43	3.24	3.78	3.58	3.61	3.57	1.91	3.15	3.82	4.07	4.68	3.92	4.13	4.44	2.59	4.22	2.00	3.09	1.88	2.39	3.66	2.91	2.79	2.54	4.18	3.54	0.05	3.30	4.45	4.61
P_2O_5	0.12	0.19	0.21	0.19	0.05	0.16	0.18	0.16	0.35	0.17	0.02	0.18	0.15	0.15	0.01	0.17	0.25	0.16	0.18	0.19	0.19	0.17	0.22	0.38	0.20	0.37	0.16	0.17	0.25	0.18	0.12	0.17
LOI	3.16	5.18	5.64	5.93	2.50	6.87	6.36	6.31	6.70	5.57	7.50	2.67	4.74	5.84	6.73	5.89	5.30	7.59	4.64	6.12	5.00	6.66	6.96	7.66	4.96	5.34	3.20	5.94	5.64	9.37	5.91	4.92
Total	100.54	99.90	98.84	100.16	100.59	100.03	98.51	100.12	100.36	100.30	100.37	99.88	100.35	100.56	100.51	100.04	100.38	99.03	99.39	100.07	99.81	100.22	100.36	99.25	100.19	98.96	100.45	98.71	101.03	100.00	100.02	100.09
FeO* wt%	5.87	4.36	5.95	5.70	5.18	6.31	5.88	6.64	5.12	4.33	4.03	3.65	4.78	5.66	7.96	4.59	4.62	3.85	4.32	5.69	5.32	5.03	7.31	6.45	6.08	8.01	6.90	5.40	4.96	0.62	9.18	5.89
S wt%	0.05	0.70	1.68	0.89	0.05	1.59	1.86	2.27	1.50	1.01	0.04	0.59	1.46	1.50	1.93	1.33	1.01	0.96	0.56	0.68	1.01	1.40	1.50	0.82	0.76	1.00	2.09	1.83	-	0.36	3.19	1.74
Trace elements (ppm)																																
Ba	383	532	349	505	484	725	641	686	282	550	475	409	515	321	443	634	358	488	349	442	332	470	659	868	477	250	789	775	345	295	711	625
Ce	62	49	44	47	50	43	79	40	79	35	68	60	36	52	37	54	43	61	44	47	61	44	41	43	50	46	36	48	57	63	22	58
Cr	33	29	43	77	23	27	38	50	28	36	13	25	28	26	25	26	34	23	29	36	29	29	106	248	30	240	28	38	39	18	42	69
Ga	38	18	16	22	20	18	19	20	24	21	15	19	21	40	37	18	23	17	18	19	17	17	21	22	21	21	23	20	4	3	17	24
Nb	12	11	10	12	11	9	11	10	11	11	12	11	11	12	10	11	11	11	12	12	12	10	10	12	10	11	11	10	10	12	10	10
Ni	2	12	21	29	1	11	17	23	19	17	1	12	10	16	18	12	16	11	15	17	16	12	31	63	14	76	17	20	12	1	22	22
Pb	187	37	47	36	259	52	1115	67	18	10	18	77	3	26	31	146	28	343	9	4	33	44	31	105	32	18	12	577	28	120	3	10
Rb	139	128	96	119	134	134	137	135	60	123	133	142	143	109	136	146	109	144	79	116	72	102	127	108	116	82	120	137	4	117	125	151
Sr	21	19	73	12	16	28	58	25	196	40	19	47	16	13	10	27	112	51	237	54	245	173	49	53	62	71	24	28	1552	183	18	48
Th	16	12	8	10	14	10	6	11	11	13	14	11	11	11	10	10	10	9	12	12	13	13	8	4	10	4	9	6	9	6	5	9
V	117	124	138	137	86	114	141	116	172	85	82	108	108	154	111	104	148	101	109	124	130	103	150	325	210	337	122	143	122	51	145	217
Y	5	13	12	13	<2	11		11	16	11	11	10	9	26	11	8	15	0	15	14	11	11	15	19	15	21	14		6		20	22
Zr	150	127	112	131	138	113	130	117	134	142	135	130	126	131	126	124	131	122	130	130	130	124	138	129	128	123	135	122	127	134	125	175
As	48	24	12	12	56	27	120	40	8	4	162	46	22	29	27	42	6	62	9	8	32	10	22	22	28	18	10	76	-	45	29	16
Zn	188	317	823	262	22	378	862	163	35	43	33	415	6	25	8	474	70	752	522	303	448	317	160	494	473	488	11	526	-	124	68	85
Cu	169	73	8	11	10	4	136	155	6	1	120	62	6	4	3	74	4	90	439	119	129	66	5	2	72	9	1	68	-	47	5	12
U	4	3	2	3	3	3	4	3	2	3	4	4	4	3	4	4	3	4	2	3	2	2	3	3	3	2	3	4	-	3	3	4
Sc	10	8	12	11	8	11	10	10	11	7	8	9	9	14	8	9	10	10	10	10	10	7	14	31	10	32	8	10	-	2	12	20
AI	97	93	55	97	97	86	61	95	75	92	98	81	91	97	97	90	83	68	51	80	54	60	90	79	74	71	90	91	42	97	92	90
CCPI	61	66	69	75	59	69	66	71	73	68	54	57	52	60	67	58	69	59	62	69	63	61	70	81	67	85	62	67	99	18	67	60
Sr/Ba	0.06	0.04	0.21	0.02	0.03	0.04	0.09	0.04	0.69	0.07	0.04	0.12	0.03	0.04	0.02	0.04	0.31	0.10	0.68	0.12	0.74	0.37	0.07	0.06	0.13	0.29	0.03	0.04	4.50	0.62	0.02	0.08

Lithology codes: And = andesite; Dior = diorite; Prph = porphyry; Pyrs = pyroclastic; Mst = mudstone.
LOI = Loss on Ignition; FeO* = total iron as FeO. Dash (-) = not determined.

AI = 100 × (MgO + K_2O)/(MgO + K_2O + CaO + Na_2O); Ishikawa et al. (1976).
CCPI = 100 × (FeO* + MgO)/(FeO* + MgO + K_2O + Na_2O); Large et al. (2001).

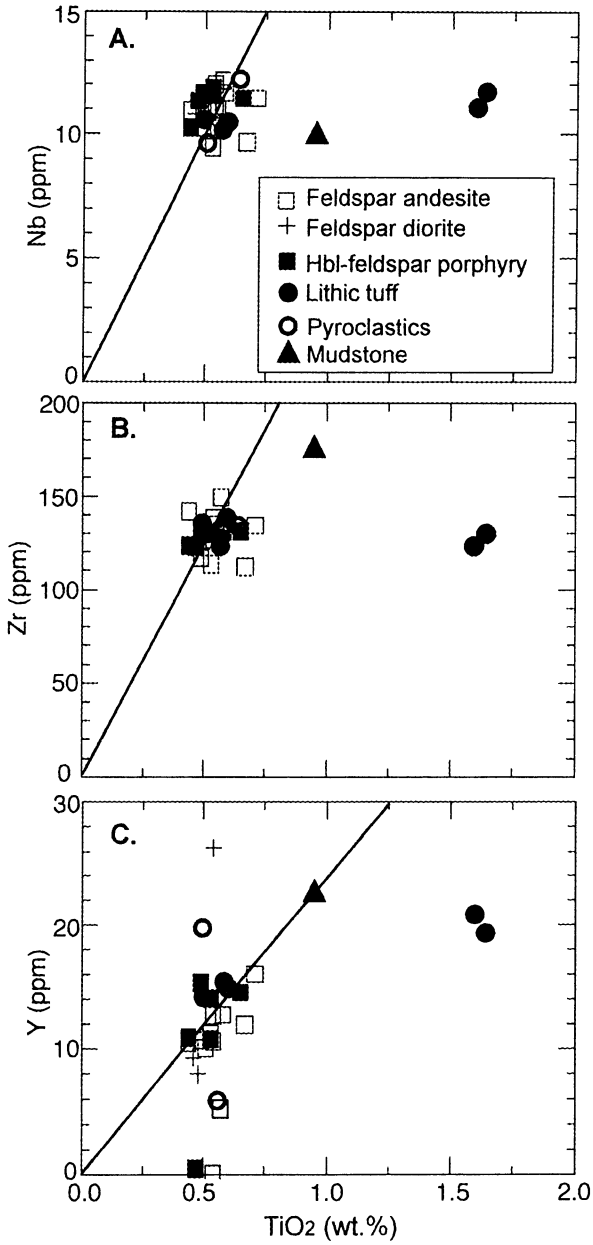

Fig. 5. Plots of immobile element abundances in the drill core samples, A–C: Nb, Zr, and Y vs.TiO_2, respectively. Linear trends are due to mass gains and losses of mobile elements (MacLean and Kranidiotis, 1987).

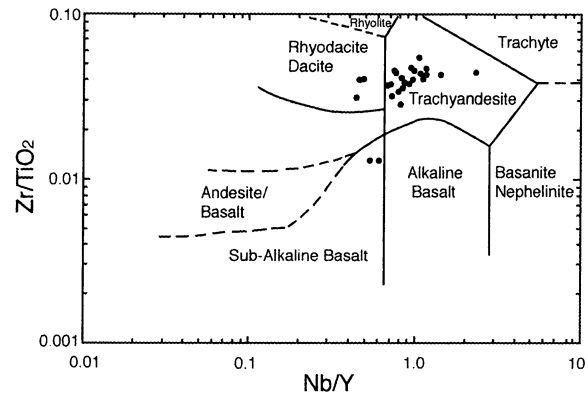

Fig. 6. Zr/TiO_2–Nb/Y diagram for the Crater Mountain igneous rocks. The Zr/TiO_2 ratio acts as a differentiation index, whereas the Nb/Y ratio serves as an alkalinity index. Diagram of Winchester and Floyd (1977).

examples of the lithotypes analyzed. Maximum abundances of Pb, As, Zn, and Cu are 1115, 162, 862, and 439 ppm respectively; total sulfur reaches 3.19 wt.%. The variability within the suite as a whole and within the individual lithotypes reflects substantial modification from original compositions due to the combined effects of silicification and hydrothermal alteration.

In contrast, Ti, Nb and Zr show little variation with respect to each other, suggesting they were relatively immobile (Fig. 5A, B). This is also the case for yttrium, although spread to lower values with respect to TiO_2 suggests limited mobility for this element in a few of the most altered samples (Fig. 5C).

Immobile elements can reflect precursor volcanic rock type and magmatic affinity, and their abundances can also be used to estimate mass and volume changes during alteration (Winchester and Floyd, 1977; Bates and Stumpfl, 1981; Stolz, 1995). The Zr/TiO_2 vs. Nb/Y discrimination diagram of Winchester and Floyd (1977; Fig. 6) shows that the samples (volcanics and intrusives) are dominantly trachyandesites, with a few rhyodacites/dacites and sub-alkaline basalts.

The samples analyzed were of six different lithotypes: feldspar andesite, diorite, quartz-hornblende-feldspar porphyry, lithic tuff, pyroclastics, and mudstone. The total destruction of all primary felsic and mafic silicate phases and their replacement by lower-density phyllosilicates, quartz, and carbonates is taken as evidence for potential mobility of the major rock-forming elements. Plots of elemental abundances against immobile species can be used to demonstrate residual enrichment or depletion of both major and trace elements, based on the model of Ague (1994). Data here were plotted against TiO_2 as the immobile species, but the results are far from conclusive. The majority of the samples are poor in TiO_2 and the range is quite restricted (0.46-0.76 wt.%) except for two lithic tuff samples with >1.6 wt.% and a mudstone sample with 0.95 wt.%.

In addition to Nb, Zr, and Y (Fig. 5), six other elements (Al_2O_3, Fe_2O_3, P_2O_5, Sc, V, and Ga; Fig. 7) show little systematic variation with TiO_2 content, with only a few samples displaced from their data clusters. These features suggest these elements were relatively immobile. This is also the case for Ce and Th, although both these elements rather more scatter than would normally be expected for truly immobile species. There is little sign of any trend towards the origin among these elements. This suggests that dilution (e.g. by SiO_2) is not a major factor in this suite, or that dilution effects have been obscured by mass losses or

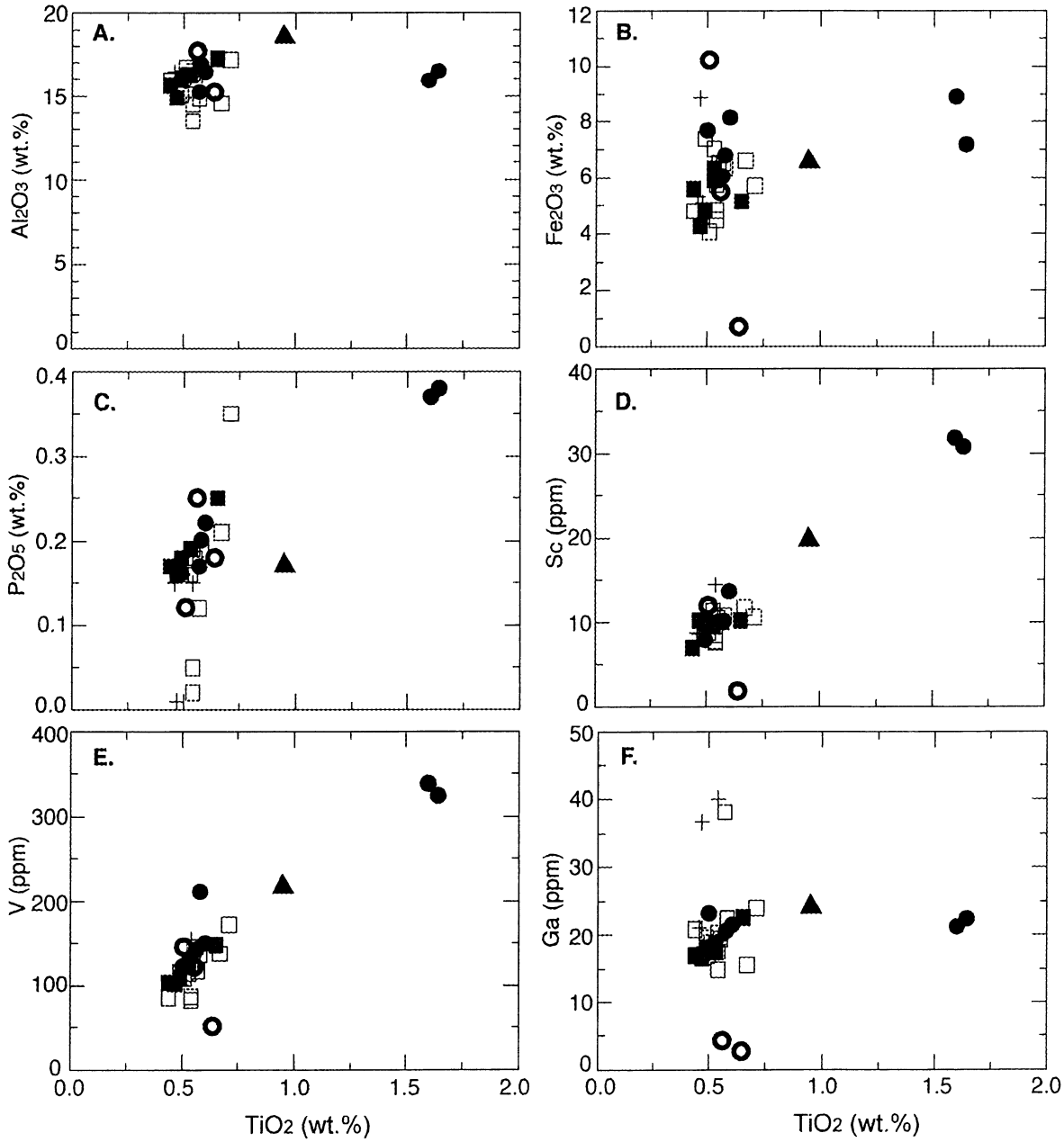

Fig. 7. Plots of (A) Al_2O_3; (B) Fe_2O_3; (C) P_2O_5; (D) Sc; (E) V; and (F) Ga abundances against TiO_2. Symbols as in Fig. 5.

gains for individual elements due to varying alteration style (e.g. for Fe, destruction of ferromagnesian minerals versus pyritization). A weak trend towards the origin for Sc and V (Fig. 7) more likely reflects the close geochemical affinity of these elements with Ti, and thus may represent original petrogenetic variation.

Elements such as CaO, Na_2O, K_2O, MgO, Ba, Sr and Rb can be expected to be mobile due to their association with easily altered phases such as feldspar and ferromagnesian minerals, and considering their abundances in alteration products. Abundances of all the above elements show considerable variation in the group of samples with restricted range in TiO_2 (Fig. 8), suggestive of mobility. However, the distributions of data show little systematic variation with LOI (assuming LOI to be a proxy for the degree of alteration). This factor, the small range in TiO_2 contents, and the lack of data for unaltered protoliths makes estimation of the direction of transfer of elements difficult. However, in general terms, it seems likely that Na_2O, CaO, Ba and Sr have been lost, whereas K_2O and Rb may be enriched. These changes reflect the complete breakdown of primary silicates and their replacement by mixtures of quartz, sericite, chlorite, K-feldspar, carbonates and sulfides during alteration under high water/rock ratio conditions. All the lithotypes show variable degree of alteration.

Sulfur contents vary significantly (0.04–3.19 wt.%), due

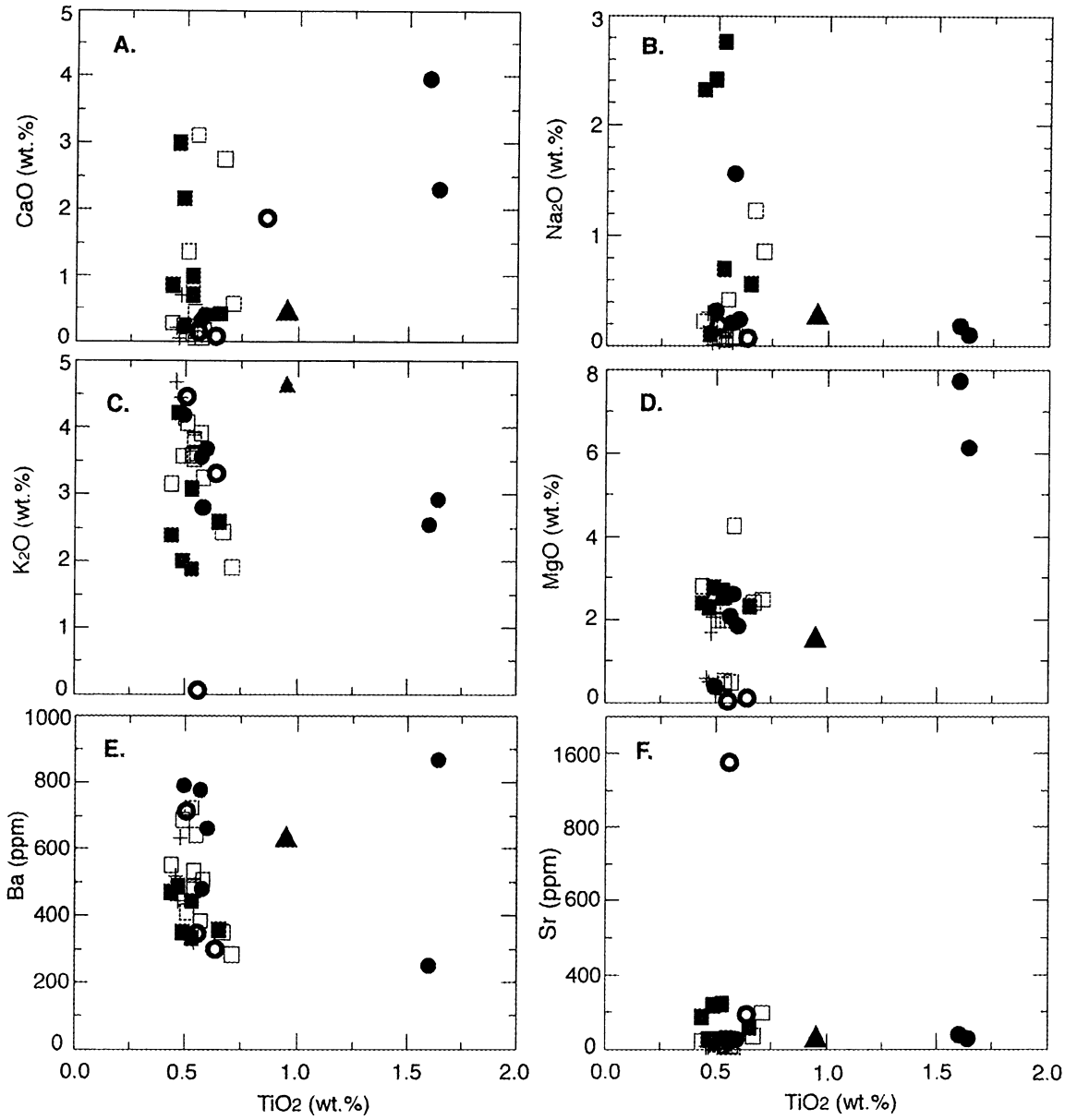

Fig. 8. Plots of (A) CaO; (B) Na_2O; (C) K_2O; (D) MgO; (E) Ba; and (F) Sr against TiO_2. Symbols as in Fig. 5.

to the presence of abundant sulfide phases, mainly replacing primary ferromagnesian minerals and Fe-bearing silicates such as chlorite and Fe-Ti oxides. Metal concentrations (i.e. Cu, Zn, As, Ni and Pb) in these samples are poorly correlated with S (Fig. 9A and B). Of this group, Zn appears to be the best pathfinder to mineralization, as the samples most enriched in zinc contain significant disseminated sulfide phases such as sphalerite and sulfosalts. The lack of correlation for the other elements presumably reflects the relative abundances of sulfide species in individual samples, including pyrite, the major sulfide species. Fe shows some correlation with S (Fig. 9C).

Alteration geochemistry

The principal geochemical dispersion patterns that characterize the main alteration types are summarized in Figs. 10 and 11. The major element variations are reflected in the values of the Ishikawa alteration index (AI = 100 × (MgO + K_2O)/(MgO + K_2O + CaO + Na_2O); Ishikawa et al., 1976). The index is generally high (AI = 71–98) but a few samples have values as low as 41 (Fig. 10). A general increase in the index across the alteration envelope reflects the extent to which feldspar has been replaced by sericite, chlorite and/or carbonate (Fig. 10.)

The chlorite-carbonate-pyrite index (CCPI = 100 × (FeOt + MgO)/(FeOt + MgO + K_2O + Na_2O); Large et al., 2001) is elevated, with values between 54 and 99, except for one

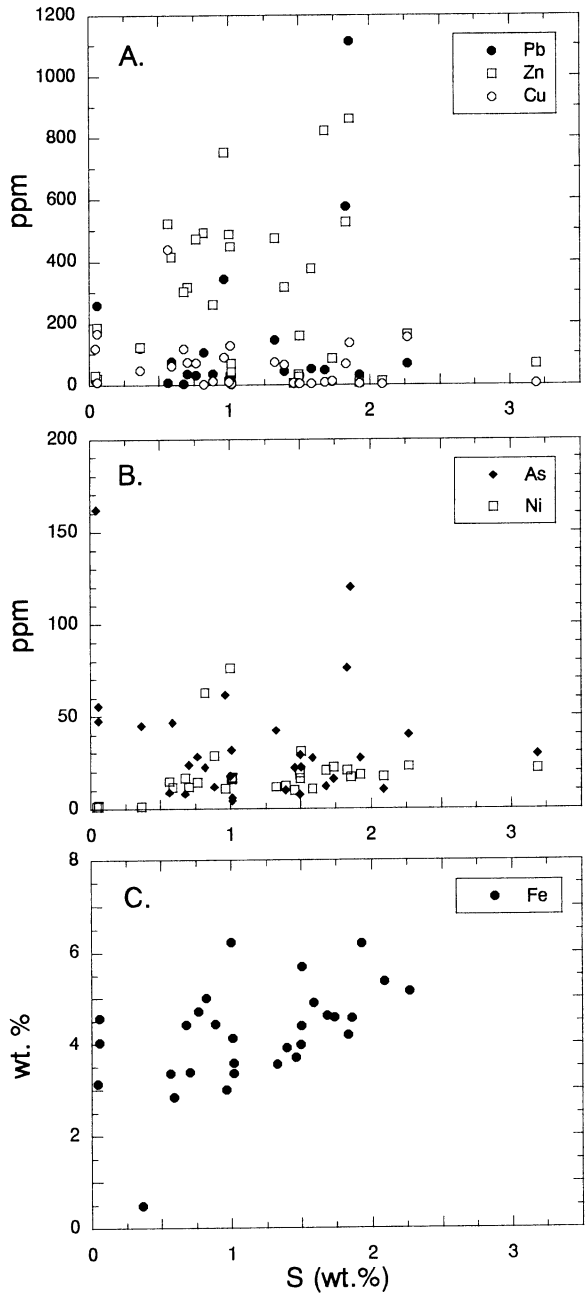

Fig. 9. Whole-rock concentrations of (A) Pb, Zn, Cu; (B) As, Ni; and (C) Fe plotted against total sulfur content (wt.%).

sample with an unusually low value of 19 (Fig. 10). The AI –CCPI plot shows relatively unaltered samples fall in the least altered box, trending toward chlorite-sericite-pyrite alteration. The least altered samples within and outside the alteration envelope have values of AI = 41 to 61 and CCPI = 63 to 99 (Fig. 10).

Reduction in Na_2O (Fig.11 A) and CaO with increasing alteration index suggest that both elements decrease in the predominant quartz-sericite ± pyrite zones. Na_2O is relatively abundant (>2 wt.%) in the hornblende-feldspar porphyry, but CaO is variable in all samples, reflecting variable carbonate concentrations. Very low Na_2O values indicate strong alteration (Barrett et al., 1993) because unaltered volcanics typically contain 2 to 5 wt.% Na_2O (Large, 1992).

K_2O abundances generally increase with increasing alteration index (Fig. 11B). The hornblende-feldspar porphyry, mudstone and pyroclastics have the greatest concentrations (4.7–5 wt.%). Hydrothermal alteration causes consistent enrichment in SiO_2, K_2O and Rb and depletion in CaO, Na_2O, P_2O_5, Sr, Ba and MnO. Concentrations of MgO, Al_2O_3, and Fe_2O_3 are dependent on the local proportions of relevant alteration minerals, whereas TiO_2 depends on the unaltered minerals. Fe_2O_3 concentrations are similar in all samples except for a single pyroclastic sample with a value as low as 0.77 wt.% (Fig. 11C). The Sr/Ba ratio is also an effective vector to ore, and measures the depletion in Sr during destruction of albite, coupled with the substitution of Ba for K in muscovite (Doyle, 2001). Ratios are lowest at AI values greater than 90, the exception being an intensely chloritized rock (Fig. 11D).

The geochemical patterns at Crater Mountain reflect contemporaneous mineralogical and textural changes accompanying volcanic-associated hydrothermal alteration and ore-associated hydrothermal alteration. This is well illustrated by the AI–CCPI plot (Fig. 10), where alteration assemblages migrate along trend lines representative of carbonatization, chloritization, sericitization and pyritic alteration (Large et al., 2001). In many cases contribution by these different alteration styles to the final chemistry become more complex approaching ore, primarily due to overprinting.

The enrichment and depletion of the elements discussed above suggests that the permeability of the rocks and movement of hydrothermal fluids is the main mechanism responsible for the movement of the elements, either locally or regionally within different lithologies. Hydrothermal alteration is more intense in the volcanic lithotypes than the intrusives. Alteration is also more intense along factures and veins in all lithotypes because these structures were conduits for the migration of hydrothermal fluids.

The entire igneous complex has experienced variable degrees of propylitic alteration associated with ore mineralization. Intense phyllic to argillic alteration occurs locally. Propylitic alteration in the weakly altered rocks is characterized by the appearance of sericite, calcite and minor chlorite in the matrix, and selective replacement of plagioclase. Phyllic (sericite–carbonate) alteration has generally resulted in almost total destruction of primary igneous mineralogy, but relict textures such as the outlines of phenocrysts are often preserved. Apatite and zircon are generally the only primary minerals which survived this alteration. The sericite typically occurs as very fine, flaky, fibrous grains, and forms intergrowths with fine-grained quartz and carbonate. Arsenical, auriferous pyrite accompanies this alteration.

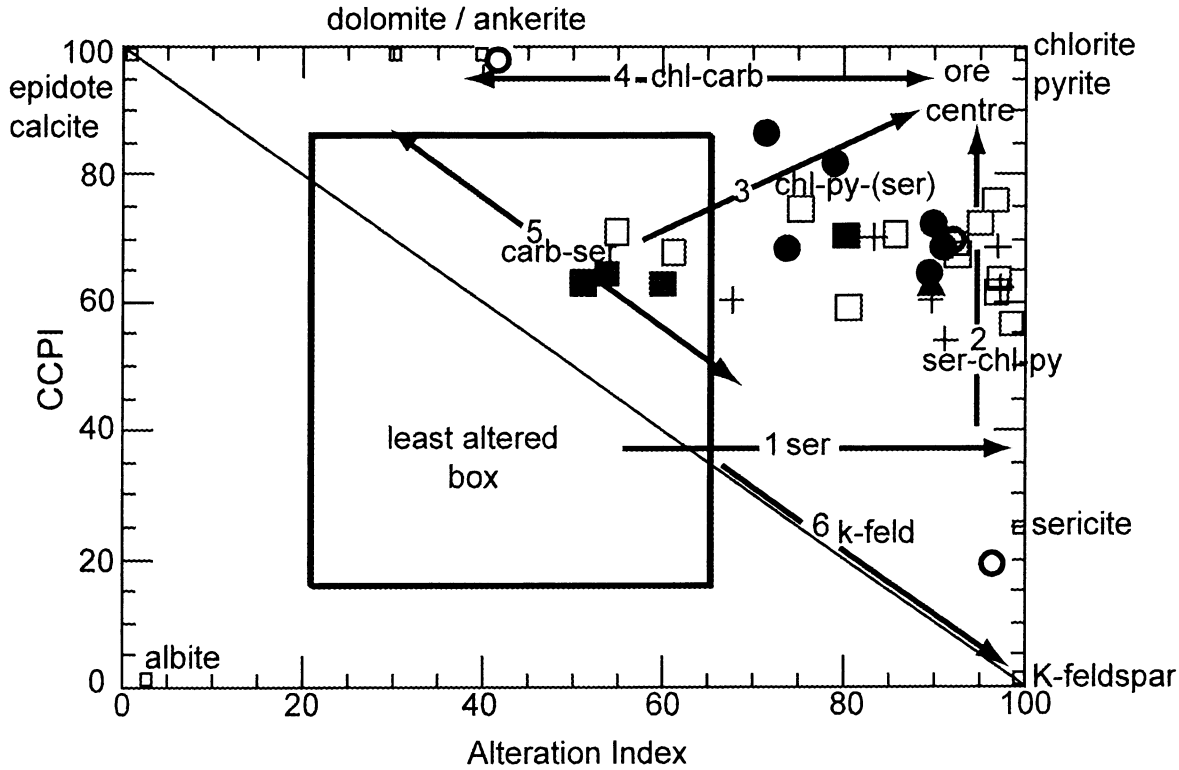

Fig. 10. Alteration box plot for altered Crater Mountain rocks using the scheme of Large et al. (2001). Fields for diagenetic alteration (lower left) and hydrothermal alteration (upper right) in the alteration box plot. The arrows show the common trends for hydrothermal alteration. Abbreviations: chl = chlorite, carb = carbonate, ser = sericite, k-feld = potassium feldspar, and py = pyrite. Symbols as in Fig. 5.

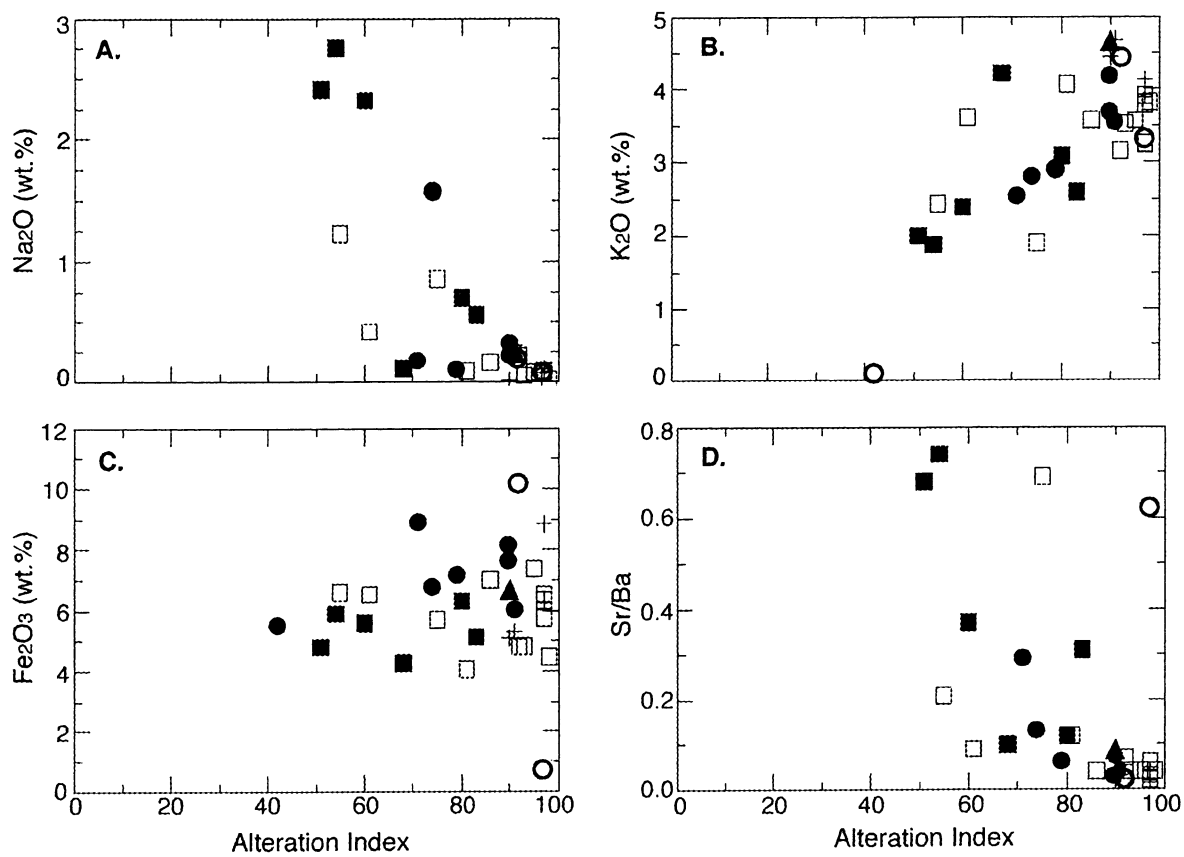

Fig. 11. Variations of (A) Na_2O, (B) K_2O, (C) Fe_2O_3 and (D) Sr/Ba vs. Ishikawa alteration index for the Crater Mountain drill core samples. Symbols as in Fig. 5.

Conclusions

Immobile trace element ratios (Zr/TiO_2–Nb/Y) indicate most samples were originally of trachyandesite composition, and the remainder were sub-alkaline basalt or rhyodacite/dacite. All of these rock types were hydrothermally altered. Increasing intensity of hydrothermal alteration at Crater Mountain is indicated by:

* Ti, Nb, Y and Zr were relatively immobile, although they are mildly variable in all lithotypes.
* Consistent enrichment in SiO_2, K_2O and Rb and depletion in CaO, Na_2O, P_2O_5, Sr, Ba and MnO. Concentrations of MgO, Al_2O_3, and Fe_2O_3 are dependent on the local proportions of relevant alteration minerals.
* Development of carbonate veining (ferroan magnesite-magnesian siderite) and carbonate flooding (dolomite-ankerite).
* Abundance of disseminated pyrite (some As-rich pyrite) and sphalerite.
* Increased abundance of carbonate, quartz and sulfide veinlets.
* Development of a K-mica (K-metasomatism) + carbonate + chlorite assemblage. Fe and Mg contents in K-mica decrease in the samples with increasing alteration. This may represent a change in Na content to muscovite/sericite (K).
* Feldspar (albite) is replaced by K-mica, carbonate ± chlorite.
* Leaching resulted in enrichment and depletion of mobile elements in all the lithotypes.
* The AI–CCPI plot indicates that all lithotypes were hydrothermally altered, and the various alterations were related to ore mineralization.

Hydrothermal chlorite–pyrite, chlorite–carbonate and quartz–sericite are the dominant alteration assemblages related to mineralization. Recognition of these alteration assemblages within unprospected areas in Crater Mountain may lead to identification of mineralized zones.

Acknowledgements

This study formed part of an M.Sc. study by S.K.N., who was funded by a Monbukagakusho MEXT scholarship. Macmin N.L granted permission to access drill core samples at the exploration site. Thanks to Andrew Kupayari and his family for their hospitality during field work.

References

Ague, J. J. 1994. Mass transfer during Barrovian metamorphism of pelites, south-central Connecticut. I: Evidence for changes in compositions and volume. *American Journal of Science*, **294**, 989-1057.

Barrett, T. J., MacLean, W. H., Cattalani, S. and Hoy, L. 1993. Massive sulfide deposits of the Noranda area, Quebec. V. The Corbet mine. *Canadian Journal of Earth Sciences*, **30**, 1934-1954.

Bates, T. F. and Stumpfl, E. F. 1981. The behaviour of so-called immobile elements in hydrothermally altered rocks associated with volcanogenic submarine-exhalative ore deposits. *Mineralium Deposita*, 16, 319 - 328.

Buckley, H. A. and Woolley, A. R. 1990. Carbonates of magnesite-siderite series from four carbonatite complexes. *Mineralogical Magazine*, **54**, 413 -418.

Doyle, M.G. 2001. Volcanic influences on hydrothermal and diagenetic alteration: Evidence from Highway-Reward, Mount Windsor Subprovince, Australia. *Economic Geology*, **96**, 133-1148.

Foster, M. D. 1962. Interpretation of the composition and a classification of chlorite. U.S. *Geol Surv Prof Pap* 414-A.

Gilbert, D. 1996. Petrology and alteration mineralogy of samples from the Nevera and Nimi prospect, Crater Mountain, PNG. *Memorandum*, pp 1-15.

Hall, D. 1994. Summary Report EL.115-Crater Mountain Papua New Guinea. *Annual report to Macmin N.L (Unpublished)*.

Ishikawa, Y., Sawaguchi, T., Iwaya, S. and Horiuchi, M. 1976. Delineation of prospecting targets for Kuroko deposits based on modes of volcanism of underlying dacite and alteration haloes. *Mining Geology*, **26**, 105-117 (in Japanese with English abstract).

Kimura, J.-I. and Yamada, Y. 1996. Evaluation of major and trace element analyses using a flux to sample ratio of two to one glass beads. *Journal of Mineralogy, Petrology and Economic Geology*, **91**, 62-72.

Johnson, R. W. 1982. Papua New Guinea. In: R.S. Thorpe (Editor), *Andesites*. Wiley, New York, NY, pp. 225-244.

Large, R. R. 1992. Australian volcanic-hosted massive sulfide deposits: Features, styles, and genetic models. *Economic Geology*, **87**, 471-510.

Large, R. R., Gemmell, J. B., Paulick, H. and Huston, D. L. 2001. The alteration box plot: A simple approach to understanding the relationship between alteration mineralogy and lithogeochemistry associated with volcanic-hosted massive sulfide deposits. *Economic Geology*, **96**, 957-971.

MacLean, W. H., and Kranidiotis, P. 1987. Immobile elements as monitors of mass transfer in hydrothermal alteration: Phelps Dodge massive sulfide gold deposit, Matagami, Quebec. *Economic Geology*, 82, 951-962.

Mason, D. R. and McDonald, J. A. 1978. Intrusive rocks and porphyry cooper occurrences of the Papua New Guinea-Solomon Islands region. *Economic Geology*, **73**, 857-877.

Noku, K. S. 2003. Geology and mineralogy of Crater Mountain deposit, Papua New Guinea: characterization and classification. Unpublished M. Sc. Thesis, Department of Geoscience, Shimane University,. 130 pp.

Pertzel, B. 1998. Petrographic descriptions for five drill core samples (Highlands, Papua New Guinea). *Memorandum, Mason Geoscience Report #* 2474, 14 pp.

Pile, J. L. and Philip, R. 1995. EL 1115 Crater Mountain annual report for the period ending 26 September 1995. *Geological Survey of Papua New Guinea Open File Report No: 95/074*.

Pile, J. L. and Philip, R. 1996. EL-1115 Crater Mountain annual report for the period ending 26 September 1996. *Geological Survey of Papua New Guinea Open File Report No: 97/023*.

Richards, J. P. 1990. Petrology and geochemistry of alkalic intrusives at the Porgera gold deposit, Papua New Guinea. *Journal of Geochemical Exploration*, **35**, 141-199.

Stolz, A. J. 1995. Geochemistry of the Mount Windsor Volcanics: Implications for the tectonic setting of Cambro-Ordovician volcanic-hosted massive sulfide mineralization in northeastern Australia. *Economic Geology*, **90**, 1080-1097.

Winchester, J. A. and Floyd, P. A. 1977. Geochemical discrimination of different magma series and their differentiation products using immobile elements. *Chemical Geology*, **20**, 325-343.

(Received: Dec. 1, 2003, Accepted: Dec. 15, 2003)

（要　旨）

Shadrach K. Noku・赤坂正秀・Barry P. Roser, 2002, パプアニューギニア、クレーターマウンテンにおける熱水変質：変質鉱物と岩石の化学組成からの証拠, 島根大学地球資源環境学研究報告, 22, 121-133.

パプアニューギニアのクレーター・マウンテン地域は1970年以来貴金属が採掘されてきた. 1999年に採掘された7箇所の岩芯は，安山岩，閃緑岩，石英長石斑岩，角閃石長石斑岩，石質凝灰岩，火砕岩，泥岩・シルト岩からなる．これらの岩石は熱水変質しており，K–雲母，炭酸塩鉱物，緑泥石，黄鉄鉱が生成している．緑泥石は火山岩類に多く，K–雲母，炭酸塩鉱物，石英は貫入岩類に多い．燐灰石とジルコンは残存鉱物として残っている．

Zr/TiO_2–Nb/Y 比は，多くの試料が初生的に粗面安山岩の化学組成であることを示す．すべての試料は熱水変質のため初生的化学組成より SiO_2，K_2O，Rb に富み，CaO，Na_2O，MgO，Ba，Sr に乏しくなっている．Ishikawa 変質指標(AI)および緑泥石－炭酸塩－黄鉄鉱指標(CCPI)は変質の程度が大きくなるに伴い，それぞれ 51–61 から 42–98 まで，および，62–66 から 18–99 まで変化する．Zn は AI が 50 から 90 のもので富む傾向があり，Zn と As は CCPI が 55 から 75 の試料で富む．Sr/Ba 比は AI が 90 以上の試料ではきわめて低い．

地球化学的パターンと変質鉱物の化学組成は鉱化作用に伴う変質作用によって生じた母岩の鉱物学的・組織的変化に対応している．